Extension to Three Dimensions of a Holographic-moiré Technique to Separate Patterns Corresponding to Components of Displacement

A combination of dual-beam holographic interferometry and moiré provides a practical solution to the problem of the optical separation of displacement components

by J.A. Gilbert, C.A. Sciammarella and S.K. Chawla

ABSTRACT—The holographic-moiré technique to obtain separate patterns for the Cartesian components of the displacement vector is extended to curved surfaces. An initial pattern which is often required for the observation of the displacement fringes is analyzed for this case. Criteria are established for the localization of this initial pattern to follow close to the contour of the object surface. A PVC pipe subjected to torsion demonstrates the proposed technique and, when analytical arguments are checked experimentally, a close correlation is observed.

List of Symbols

a = distance between points P and M on object surface
d, d' = displacement magnitudes
$\underline{d}, \underline{d}', \underline{d}_t$ = displacement vectors
d_o = outer diameter of the pipe
d_I = inner diameter of the pipe
$e_1, e_1' e_2, e_R$ = propagation vector
$\underline{g}$ = sensitivity vector
n = fringe-order number
$\underline{n}_p$ = plate normal
$\underline{n}_s$ = unit vector
C = rotation center
D = distance between model and photographic plate
E = Young's modulus
L = length of pipe
M,O,P,P′,P$_1$,P$_1$′,P$_2$,Q,Q′ = points under consideration
M_t = applied torque
$(R_p, \theta_p), (R_{\bar{p}}, \theta_{\bar{p}}), (R_c, \theta_c)$ = polar coordinates
$(R_R, \theta_R), (R_m, \theta_m), (R_{\bar{m}}, \theta_{\bar{m}})$
$(U, V, W), (U_r, U_\theta, U_z)$ = displacement components
$(X, Y, Z), (r, \theta, z)$ = coordinates
Z_c = distance between photographic plate and rotation center
α = sensitivity angle
β = angle of rotation of photographic plate
δ, δ' = angular phase change
δ_M = fringe spacing
θ^* = angle of twist per unit length
$\theta_T, \theta_R, \theta_P$ = angles
λ = wavelength of laser light
ν = Poisson's ratio
$\phi(z)$ = angle of twist
$\Delta\theta_p, \Delta\theta_M$ = incremental angles

J.A. Gilbert is Professor, College of Engineering and Applied Science, University of Wisconsin, Milwaukee, WI 53201. C.A. Sciammarella and S.K. Chawla are associated with the Illinois Institute of Technology, Chicago, IL 60616.

Revised version of manuscript received: October 21, 1977.

Introduction

Holography and holographic interferometry are beginning to have an impact on today's technology. Interest has spread from the research laboratory to industry, where a practical approach is required to make any technique readily acceptable. The holographic-moiré method offers potential in this respect.

A double-beam illumination technique to separate components of displacement was first suggested by Butters[1] and Boone.[2] It was shown that the displacement vector of every model point could be projected into a single plane if the doubly exposed holograms, corresponding to two different illuminations, were optically superimposed by reconstruction from a common point of observation.

This approach worked in theory; however, in practice, the superposition of these two fringe patterns was often difficult or impossible to observe. The orientation, gradient and spacing of the two arbitrary fringe systems did not always lend themselves to the formation of a moiré. Localization also presented a problem.

To circumvent these difficulties, a rigid-body motion was imparted to the model to create more fringes in each component pattern.[3,4] This additional phase change was common to each component pattern and disappeared in the final superposition.

The latter solved the problem to some extent; however,

imparting motion other than the actual displacement to the model itself was not acceptable from a practical standpoint. A more desirable solution was presented by the authors who introduced an additional fringe system without disturbing the model.[5] This was accomplished by rotating the photographic plate between exposures. This additional degree of freedom made it possible to optically superimpose holograms, to apply spatial filtering techniques, and to control fringe localization. The method was shown to be applicable throughout the entire holographic range and has been applied on interior planes of transparent bodies.[6]

All of the experimental studies in the references listed have applied the holographic-moiré technique to plane surfaces. This paper explores the possibility of extending the method to treat curved surfaces. A discussion of the general equations governing the displacement field is followed by a derivation for the localization and spacing of the initial pattern on curved surfaces. This pattern is often required for the observation of the displacement fringes. Analytical arguments are checked by considering a section of a PVC pipe subjected to pure torsion.

Holographic-moiré Theory for Curved Surfaces

Figure 1 shows a point P on a diffusely reflecting surface whose local normal is $\underline{n}_s$. The surface is illuminated by two beams whose angle bisector is $\underline{n}$. The propagation vectors in the direction of each illumination are $\underline{e}_1$ and $\underline{e}_1'$, respectively. The point P is observed from an observation point corresponding to the propagation vector $\underline{e}_2$ which has been aligned with $\underline{n}$ for convenience only. When the point P experiences a displacement $\underline{d}$ between exposures, two holographic fringe systems are observed which are characterized by,

$$\delta = (\underline{e}_1 - \underline{e}_2) \cdot \underline{d} \tag{1}$$

and

$$\delta = (\underline{e}_1' - \underline{e}_2) \cdot \underline{d} \tag{2}$$

where δ and δ' are the phase changes experienced by the point P during the displacement.

These two component patterns are simultaneously observed and, theoretically, are optically superimposed to form a moiré pattern which represents the net phase change between them. That is, the moiré is given by

$$\delta - \delta' = (\underline{e}_1 - \underline{e}_1') \cdot \underline{d} = \underline{g} \cdot \underline{d} = \underline{d}' \tag{3}$$

where $\underline{g}$ is often referred to as a sensitivity vector and $\underline{d}'$ is the projected displacement component which is perpendicular to $\underline{n}$ as shown in Fig. 1. The magnitude of $\underline{d}'$ is directly dependent upon 2α, the angle between the two illuminating beams. Converting eq (3) from angular to linear phase,

$$d' = \frac{n\lambda}{2 \sin \alpha} \tag{4}$$

where n is the fringe order number and λ is the wavelength of the incident light.

For collimated illuminations, the sensitivity vector $\underline{g}$ remains constant over the full-field and the displacement is projected into a single plane. In the case of a flat surface, when $\underline{n}_s$ coincides with $\underline{n}$, θ_T is equal to zero and the displacement $\underline{d}'$ becomes $\underline{d}_T$ which is referred to as normal to the line of sight or 'in-plane'.

As noted in Ref. 5, localization problems or fringe characteristics such as spacing, gradient and orientation often make the optical subtraction, or moiré, or the component patterns difficult or impossible to observe. To circumvent this difficulty, the photographic plate is rotated between exposures. This generates an initial pattern, representing a fictitious displacement, with high fringe density. Since the phase change initiated by this rotation is common to each illumination, eq (4) remains valid.

In addition to creating component patterns with high fringe density capable of producing a moiré, the initial pattern can be used to control the fringe localization of the component patterns. This may be necessary since the displacement of the object gives rise to holographic patterns whose localization depends upon the type of displacement initiated between exposures and the geometry of the optical system. Therefore, even if the component patterns have a sufficient number of fringes to produce mutual interference, their localization planes may differ to such an extent that simultaneous reconstruction is impossible. If, however, the rotation of the photographic plate produces an initial pattern which is localized on the object surface and the phase change corresponding to this rotation is large as compared to that produced by the deformation, the localization of the resulting component patterns approaches the object surface. Holographic-moiré displacement fringes result and when the moiré and the object are simultaneously reconstructed, the observation-projection theorem[7,8] ensures that the interference observed corresponds to the actual displacement of points on the object surface.

The section which follows analyzes the formation of the initial pattern on curved surfaces.

Formation of the Initial Pattern on Arbitrary Three-dimensional Surfaces

Figure 2 shows the system of coordinates used in this derivation. A cross section of a cylindrical object is shown,

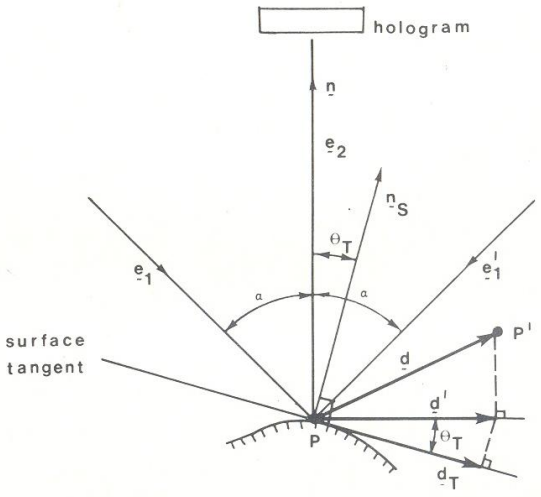

Fig. 1—Displacement analysis

although the conclusions reached herein are of general nature and are not restricted to any shape in particular. HH and H′H′ are the initial and final positions of the holographic plate, respectively. The plate is rotated around an axis of rotation perpendicular to the plane of the figure that passes through a point C selected such that, as determined in Ref. 5

$$Z_c = D\,(1 - \cos\theta_R) \tag{5}$$

where Z_c is the abscissa of the center of rotation, D the distance of the point of localization to the holographic plate, and θ_R is the angle defining the reference beam.

Localization now occurs at the point M on the surface of the cylinder and all the homologous rays corresponding to point M will intersect there. Let us consider a point P on the surface. An initial exposure allows light corresponding to the propagation vector e_2, diffused from point P, to interfere with the reference beam at point P_1 on the holographic plate. After the plate is rotated, a second exposure is taken, and the propagation vector e_2 intersects the plate at P_2.

Let us assume that the hologram is developed, placed back in its rotated position and then reconstructed. The reconstructed beam P_2P goes back to the point P. The point P_1 which is at P_1' is also reconstructed and the beam $P_1'P'$ intersects P_1P at P'. We will show that P' is located near P, and that the region of maximum contrast of the interference fringes produced by the rotation of the plate is near the surface of the object.

To prove this point we can make use of the equations derived by Champagne.[9]

In the present case, these equations can be written

$$\frac{1}{R_{\bar{P}}} = \frac{1}{R_c} + \left(\frac{1}{R_P} - \frac{1}{R_R}\right) \tag{6}$$

and

$$\sin\theta_{\bar{P}} = \sin\theta_c \pm (\sin\theta_P - \sin\theta_R) \tag{7}$$

The above equations give the image polar coordinates $R_{\bar{P}}$ and $\theta_{\bar{P}}$ with respect to the origin of coordinates O, in terms of the coordinates R_P and θ_P for the object, R_c and θ_c for the reconstruction source, and R_R and θ_R for reference source. If $R_{\bar{P}}$ is positive, the image is virtual while, if $R_{\bar{P}}$ is negative, the image is real. The plus sign is associated with the primary wave and the minus sign with the conjugate wave.

In the case under analysis, we have rotated the plate around a given axis such that the localization surface has a point in common with the object. When we reconstruct the rotated hologram, it is possible to determine the final position of the reconstructed object by applying eqs (6) and (7) and by considering the motion of the origin of coordinates.

From eq (6), in view of the fact that $R_c = \infty$ and $R_R = \infty$, we obtain

$$R_{\bar{P}} = R_P \tag{8}$$

Although the plate has been rotated, and the reference beam has been kept constant, eq (7) can be applied to obtain the value of $\theta_{\bar{P}}$ with respect to the rotated plate normal. We replace in eq (7)

$$\theta_c = \theta_R - \beta \tag{9}$$

where β is the angle of rotation of the plate and we obtain

$$\sin\theta'_{\bar{P}} = \sin(\theta_R - \beta) + \sin\theta_P - \sin\theta_R \tag{10}$$

where the prime indicates angles referred to the rotated coordinates, which can be simplified to

$$\sin\theta'_{\bar{P}} = \sin\theta_P - \beta\cos\theta_R \tag{11}$$

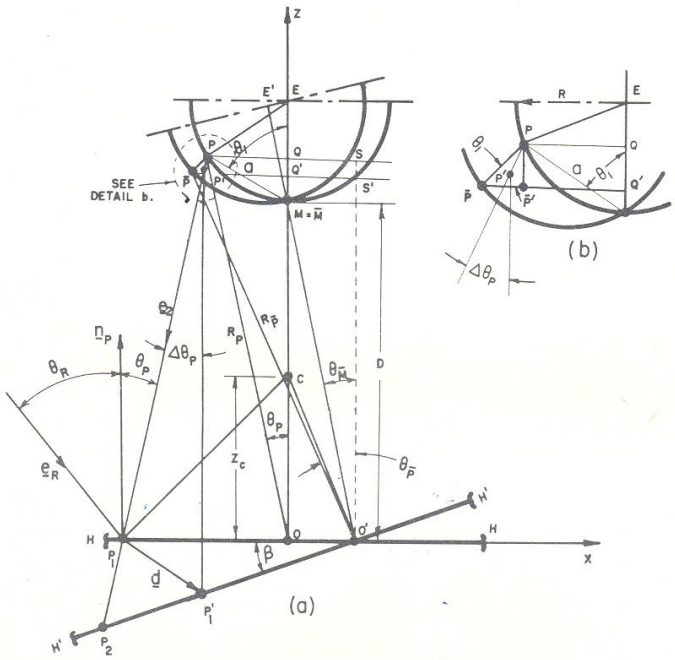

Fig. 2—Localization study

since β is a very small angle.

Let us consider point M. For point M, $\theta_M = 0$, by applying eq (11), for small angles.

$$\theta'_{\bar{M}} = -\beta \cos \theta_R \tag{12a}$$

and adding the angle rotated by the plate normal

$$\theta_{\bar{M}} = \beta - \beta \cos \theta_R \tag{12b}$$

where $\theta_{\bar{M}}$ indicates the value of the angular coordinate with respect to the nonrotated system of axis. Point O has moved by the amount

$$OO' = Z_c\beta = D(1 - \cos \theta_R)\,\beta \tag{13}$$

The final position of M can be obtained from the computed coordinate $\theta_{\bar{M}}$ and

$$R_M = R_{\bar{M}} \tag{14}$$

We can see, Fig. 2, that if we combine the simultaneous effect of the displacement of the origin of coordinates given by eq (13) and the effect of the rotation of the plate given by eq [12(b)], M = $\bar{\text{M}}$. The homologous ray defined by

$$\Delta\theta_M = \beta(1 - \cos \theta_R) \tag{15}$$

also goes through point M.

If we consider a point P, from eq (11) we can obtain

$$\sin \theta'_{\bar{P}} - \sin \theta_P = -\beta \cos \theta_R \tag{16}$$

or also

$$2 \cos \frac{\theta_P + \theta'_{\bar{P}}}{2} \sin \frac{\theta'_{\bar{P}} - \theta_P}{2} = -\beta \cos \theta_R \tag{17}$$

The above can be written

$$\sin \frac{\theta'_{\bar{P}} - \theta_P}{2} = -\frac{\beta \cos \theta_R}{2 \cos \theta_P} \tag{18}$$

if we assume that the difference between the two angles is small and therefore

$$\frac{\theta_P + \theta'_{\bar{P}}}{2} = \theta_P \tag{19}$$

from eq (18) we obtain

$$\theta'_{\bar{P}} = \theta_P - 2 \text{ arc sin } \frac{\beta \cos \theta_R}{2 \cos \theta_P} \tag{20}$$

and taking into consideration that we are dealing with a small angle, we write eq (20),

$$\theta'_{\bar{P}} = \theta_P - \frac{\beta \cos \theta_R}{\cos \theta_P} \tag{21}$$

Finally with respect to the nonrotated coordinate system

$$\theta_{\bar{P}} = \theta_P + \beta\,[1 - \frac{\cos \theta_R}{\cos \theta_P}] \tag{22}$$

or

$$\theta_{\bar{P}} = \theta_P + \Delta\theta_P \tag{23}$$

where

$$\Delta\theta_P = \frac{\beta}{\cos \theta_P}\,[\cos \theta_P - \cos \theta_R] \tag{24}$$

which agrees with eq (18) of Ref. 6. We can show that the effect of the rotation of the plate on the reconstructed object is equivalent to a fictitious rotation of the object around a rotation axis going through M, the magnitude of the rotation being $\beta(1 - \cos \theta_R)$. To locate $\bar{\text{P}}$, position of the reconstructed point, we take

$$P\bar{P} = a\,\beta\,(1 - \cos \theta_R) \tag{25}$$

the value of

$$\sin \theta_{\bar{P}} = \frac{\bar{P}\bar{P}' + \bar{P}'Q' + Q'S'}{O'\bar{P}} \tag{26}$$

but

$$\overline{P\bar{P}'} = P\bar{P} \cos \theta_1 = a\,\beta(1 - \cos \theta_R) \cos \theta_1 \tag{27}$$

also

$$\overline{\bar{P}'Q'} = PQ \tag{28}$$

From eq (13) and Fig. 2

$$Q'S' = OO' = \beta(1 - \cos \theta_R)D \tag{29}$$

Replacing in eq (26) and taking into consideration that $O'\bar{P} = OP$, we get

$$\sin \theta_{\bar{P}} = \sin \theta_P + \beta \frac{(1 - \cos \theta_R)\,(a \cos \theta_1 + D)}{OP} \tag{30}$$

but

$$OQ = a \cos \theta_1 + D \tag{31}$$

consequently

$$\sin \theta_{\bar{P}} - \sin \theta_P = \beta\,(1 - \cos \theta_R)\,\frac{OQ}{OP} \tag{32}$$

then

$$\sin \theta_{\bar{P}} - \sin \theta_P = \beta(1 - \cos \theta_R) \cos \theta_P \tag{33}$$

Following the same steps taken to derive eq (21), we get

$$\theta_{\bar{P}} = \theta_P + \beta(1 - \cos \theta_R) \tag{34}$$

then

$$\overline{\Delta\theta}_P = \theta_{\bar{P}} - \theta_P = \beta(1 - \cos \theta_R) \tag{35}$$

We can see that eqs (24) and (35) do not provide exactly the same angular coordinate.

Subtracting eq (24) from eq (35) we get

$$\overline{\Delta\theta}_P - \Delta\theta_P = \beta\,\frac{[\cos \theta_R - \cos \theta_R \cos \theta_P]}{\cos \theta_P} \tag{36}$$

For small values of θ_P, that is, for points not far from the fictitious center of rotation, the difference is practically zero. Let us consider the point on object farthest away from the apparent rotation center. If we assume that

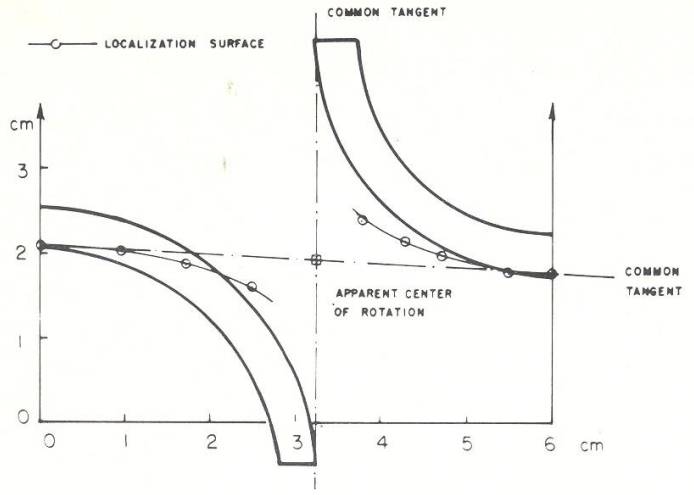

Fig. 3—Comparison of localization surface with model surface

$D = L$, where L is the maximum dimension of the object parallel to the plate, in the present case L is the outside diameter. Assuming that the apparent center of rotation is located at $L/2$

$$\sin\theta_P = \frac{\frac{L}{2}}{\sqrt{10}\,\frac{L}{2}} = 0.316;\quad \cos\theta_P = \frac{\frac{3L}{2}}{\sqrt{10}\,\frac{L}{2}} = \frac{3}{\sqrt{10}} \tag{37}$$

for the point farthest away from the apparent rotation center. The values of θ_R are chosen as large as feasible, for example if $\theta_R = 60$, then

$$\Delta\theta_P' - \Delta\theta_P = \beta\,\frac{.5 - .5 \times .95}{.95} = \beta\ .026 \tag{38}$$

If we assume $\beta = 10$ min of arc, the error in the angular coordinate is

$$\text{Error ang. coord.} = \frac{.0029 \times .026}{0.52359} \times 100 = .0144 \text{ percent}$$

For all practical purposes, the effect of the rotation of the plate is equivalent to an apparent rotation of the object around a center of rotation located in its surface neighborhood.

We can look at this problem in the following way. By rotating the plate around the center of rotation C, we are rotating the reconstructed image around the point M; however, in view of the fact that we keep the reference beam constant, there are certain aberrations of the reconstructed object, and these aberrations explain the difference between the results of eqs (24) and (35).

The preceding derivation can be utilized to obtain important conclusions concerning the localization surfaces of the fringes produced by rotating the holographic plate. The phenomenon of localization of holographic fringes arises from the fact that there are two extended partially coherent sources that interact and the localization surfaces are determined by the relative positions of these two sources. We have shown that to a high degree of approximation for very small rotations, the relative motion between the two images generated by the rotation of the plate is equivalent to a rotation of the object around an axis parallel to the plate and going through a point of the object. Under such circumstances as shown in Ref. 10, when an object rotates around an axis normal to the direction of observation, the resulting fringes are localized in the neighborhood of the object. To check the above conclusions, numerous and careful experiments have been carried out with cylindrical surfaces and with a concave ellipsoidal surface. To obtain the surface of fringe localization, the following technique was applied. By utilizing the conjugate beam, the real images of the object were reconstructed. A plate with an engraved grating was utilized to obtain the localization surface by means of the parallax technique. A simple loupe focused on the grating provided the means of observing the fringes. The localization surface was determined by eliminating the parallax between the grating and the fringes. The plate was supported in a sliding carriage with an index moving on a scale divided in mm. Measurements were found to be repeatable to one mm. In all cases it was found that the fringes localize in the neighborhood of the surface and follow the general shape of the surface. Figure 3 illustrates an example of application. Two half cylinders were utilized as objects and arranged as shown. Equation (5) was utilized to compute Z_c to localize the fringes in a tangent plane common to the two surfaces. The apparent center of rotation was a point midway between the two cylindrical surfaces. The fringe-localization surface coincides with the cylindrical surfaces at the tangency points and then departs from the cylindrical surface as the slope of the surfaces increases. The same behavior has been observed in cylindrical surfaces rotated around the generatrix located in the symmetry axis.

The fringes in the initial pattern are parallel to the axis of rotation with pitch δ_M, given by,

$$\delta_M = \frac{\lambda}{\beta(\cos\theta_P - \cos\theta_R)} \tag{39}$$

Note that δ_M is independent of the direction of illumination. Furthermore, when R (radius of the cylinder) is much smaller than D, the variation in θ_P is small and the fringe spacing approximately only depends upon θ_R.

Equation (39) has been experimentally verified for flat surfaces.[5] Similar experimental data taken from curved surfaces show eq (39) to be a universal relationship.

Although this particular discussion has dealt with a cylindrical surface, similar arguments can be constructed for other three-dimensional surfaces. In general, the localization will be close to the surface providing that the center of rotation is chosen in accordance with eq (5) so that the fringes are forced to localize at one point of the surface.

Thus, the technique of generating an initial system of fringes by means of plate rotation between exposures has universal application to separate components of displacement.

Experimental

The model used to demonstrate that the holographic-moiré method is applicable to curved surfaces is shown in Fig. 4. The geometrical parameters and the material properties of the pipe are listed. A Cartesian and a cylindrical coordinate system are also shown in the figure. The pipe is rigidly fixed at Z/L equals zero and a torque M_T is applied at Z/L equal to one, to produce a state of pure torsion.

Figure 5 shows the experimental setup along with the appropriate geometrical parameters used in the study. Axes corresponding to those shown in Fig. 4 are assigned to the model. The coordinate of C was chosen in accordance with eq (5) to force localization of the initial pattern to occur at the model point $(X, Y, Z) = (0, d_o/2, L/2)$ or $(r, \theta, Z) = (d_0/2, \pi/2, L/2)$. The model was illuminated with two collimated light beams parallel to the XY plane of the Cartesian coordinate system. The Y axis formed the angle bisector of the illuminations and each beam subtended an angle α with respect to this direction. The region chosen for this study was $0.4 \leq Z/L \leq 0.6$. Throughout this region the displacement was projected parallel to the XZ plane in the X direction. If we call (U, V, W) the displacement components corresponding to (X, Y, Z), the holographic-moiré pattern observed corresponds to U and is given by eq (4) as,

$$U = \frac{n\lambda}{2 \sin \alpha} \tag{40}$$

An initial exposure was taken of the unloaded pipe. The torque was applied to the model and the photographic plate was rotated through the angle β around an axis parallel to X, passing through C. The loaded state was then superimposed on the photographic plate with a second exposure. When the developed hologram was reconstructed, the holographic-moiré pattern shown in Fig. 6(a) was observed. This pattern was optically filtered, Fig. 6(c), to sharpen fringe contrast and to eliminate the component patterns from the moiré. Note that, in both patterns, no information was obtained in the shadow region. That is, for $|X/D| \geq 0.47$, the two illuminations did not overlap. This restriction on the method imposed by surface geometry can be minimized at the expense of sensitivity by making the angle 2α small.

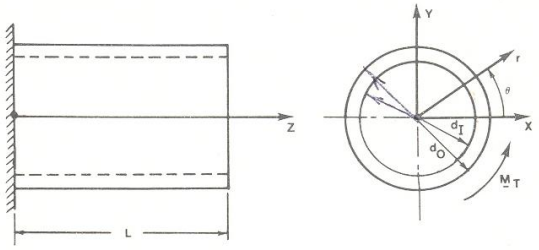

L = 16.25 in. = 0.4128 m
d_O = 1.91 in. = 0.0485 m
d_I = 1.60 in. = 0.0406 m

M_T = 3.48 lb-in. = 0.393 N-m
E = 4.00 x 10^5 psi = 27.58 x 10^5 kPa
ν = 0.37

Fig. 4—The model under study

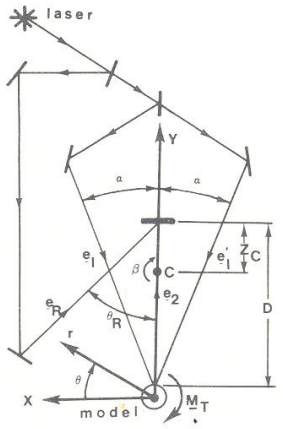

α = 20.8°
β = 4.5 arc min.
θ_R = 45°
Z_C = 6.92 in. = 0.176 m
D = 24.00 in. = 0.610 m
M_T = 3.48 lb-in. = 0.393 N-m

Fig. 5—The experimental setup

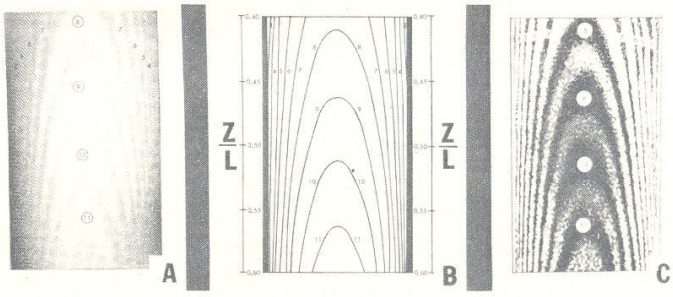

Fig. 6—U-displacement component : (a) unfiltered holographic moiré; (b) theoretical pattern; (c) filtered holographic moiré

The technique can then be applied to analyze virtually any surface which could ordinarily be illuminated with a single beam.

It is desirable to compare this experimental pattern to its theoretical counterpart. To this end, the transformation from the cylindrical to the Cartesian coordinate system shown in Figs. 4 and 5, takes the form,

$$\begin{bmatrix} \cos\theta & -\sin\theta & 0 \\ \sin\theta & \cos\theta & 0 \\ 0 & 0 & 1 \end{bmatrix} \begin{bmatrix} U_r \\ U_\theta \\ U_z \end{bmatrix} = \begin{bmatrix} U \\ V \\ W \end{bmatrix} \tag{41}$$

where (U,V,W) and (U_r,U_θ,U_z) are the displacement components corresponding to (X,Y,Z) and (r,θ,Z), respectively.

For pure torsion, the displacement on the outer surface of the pipe is,

$$U_r = U_z = 0 \quad \text{and} \quad U_\theta = \frac{d_0}{2}\phi(Z) \tag{42}$$

where d_0 is the outer diameter of the pipe and $\phi(Z)$ is the angle of twist. From eq (41),

$$U = -U_\theta \sin\theta = -\frac{d_0}{2}\phi(Z)\sin\theta \tag{43}$$

The angle of twist per unit length is given by Ref. 11

$$\theta^* = \frac{64M_T(1+\nu)}{\pi[d_0^4 - d_i^4]E} \tag{44}$$

where d_i is the inner diameter of the pipe, ν is the Poisson's ratio and E is the Young's modulus. By definition,

$$\phi(Z) = Z\theta^* \tag{45}$$

Substituting eq (44) into eq (45) and the result into eq (43),

$$U = -\frac{32d_0 M_T(1+\nu)}{\pi[d_0^4 - d_i^4]E}\{Z\sin\theta\} \tag{46}$$

Equating eqs (40) and (45) and solving for n,

$$n = -\frac{64d_0 M_T(1+\nu)\sin\alpha}{\lambda\pi[d_0^4 - d_i^4]E}\{Z\sin\theta\} \tag{47}$$

Using $\lambda = 5145 \times 10^{-8}$ cm and the information included on Figs. 4 and 5, n can be plotted in the region of interest as shown in Fig. 6(b). A visual comparison of Figs. 6(a) and 6(c) with Fig. 6(b) shows a close correlation between the experimental and theoretical patterns; however, further study is necessary to verify this observation. To this end, Fig. 7 compares the experimental and theoretical data along the section $Z/L = 0.5$. This confirms that the two patterns agree to within reasonable experimental error.

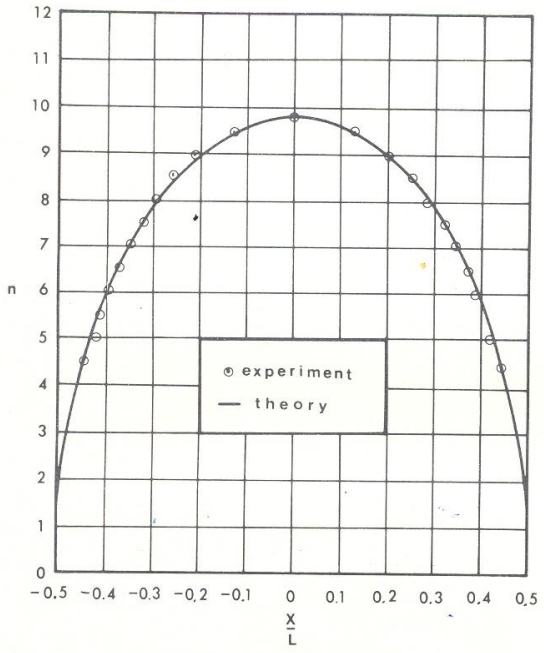

Fig. 7—Results along $Z/L = 0.50$

Conclusions

The problem of separating a single component of the displacement vector with holographic interferometry has been solved for curved surfaces. The solution is a practical one and requires only simple devices. Techniques to obtain derivatives and to suppress speckle noise are currently under investigation by the authors.

Acknowledgment

This investigation was supported by National Science Foundation through Grant No. NSF-ENG 75-1110. The authors wish to thank C.J. Astill for his continuous encouragement.

References

1. Butters, J.N., "Applications of Holography to Instrument Diaphragm Deformations and Associated Topics," The Engineering Uses of Holography, E.R. Robertson and J.M. Harvey, eds., Cambridge Univ. Press, London, New York (1970).
2. Boone, P.M., "Holographic Determination of In-Plane Deformation," Opt. Tech., **2** (1970).
3. Ebbeni, J., "A Moiré-Holographic Method to Determine the State of Deformation of a Diffusing Object," Presented 5th Int. Cong. Exp. Stress Anal., Udine, Italy (1974).
4. Hung, Y.Y. and Taylor, C.E., "Measurement of Surface Displacements Normal to the Line of Sight by Holo-Moiré Interferometry," J. Appl. Mech., **42** (1975).
5. Sciammarella, C.A. and Gilbert, J.A., "A Holographic-moiré Technique to Obtain Separate Patterns for Components of Displacement," EXPERIMENTAL MECHANICS, **16** (6), 215-220 (Jun. 1976).
6. Sciammarella, C.A. and Gilbert, J.A., "Holographic Interferometry Applied to the Measurement of Displacements of the Interior Planes of Transparent Bodies," Appl. Opt., **15** (1976).
7. Stetson, K.A., "The Argument of the Fringe Function in Hologram Interferometry of General Deformations," Optik, **33** (1970).
8. Stetson, K.A., "Fringe Interpretation for Hologram Interferometry of Rigid-Body Motions and Homogeneous Deformations," J. Opt. Soc. Am., **64** (1974).
9. Champagne, E.B., "Non Paraxial Imaging, Magnification, and Aberations Properties of Holography," J. Opt. Soc. Am., **57** (Jan. 1967).
10. Vienot J. CH. et al, "Hologram Interferometry: Surface Displacement Fringe Analysis as an Approach to the Study of Mechanical Strains and other Applications to the Determinations of Anisotropy in Transparent Objects," The Engineering Uses of Holography, E.R. Robertson and J.M. Harvey, eds., Cambridge Univ. Press, London, New York (1970).
11. Timoshenko, S., Strength of Materials, D. Van Nostrand Co., New York (1940).